

# Single-Shot Object Detection with Enriched Semantics

Zhishuai Zhang<sup>1</sup> Siyuan Qiao<sup>1</sup> Cihang Xie<sup>1</sup> Wei Shen<sup>1,2</sup> Bo Wang<sup>3</sup> Alan L. Yuille<sup>1</sup>  
Johns Hopkins University<sup>1</sup> Shanghai University<sup>2</sup> Hikvision Research<sup>3</sup>

zhshuai.zhang@gmail.com

siyuan.qiao@jhu.edu

cihangxie306@gmail.com

wei.shen@t.shu.edu.cn

wangbo.yunze@gmail.com

alan.yuille@jhu.edu

## Abstract

*We propose a novel single shot object detection network named Detection with Enriched Semantics (DES). Our motivation is to enrich the semantics of object detection features within a typical deep detector, by a semantic segmentation branch and a global activation module. The segmentation branch is supervised by weak segmentation ground-truth, i.e., no extra annotation is required. In conjunction with that, we employ a global activation module which learns relationship between channels and object classes in a self-supervised manner. Comprehensive experimental results on both PASCAL VOC and MS COCO detection datasets demonstrate the effectiveness of the proposed method. In particular, with a VGG16 based DES, we achieve an mAP of 81.7 on VOC2007 test and an mAP of 32.8 on COCO test-dev with an inference speed of 31.5 milliseconds per image on a Titan Xp GPU. With a lower resolution version, we achieve an mAP of 79.7 on VOC2007 with an inference speed of 13.0 milliseconds per image.*

## 1. Introduction

With the emergence of deep neural networks, computer vision has been improved significantly in many aspects such as image classification [11, 13, 15, 24, 27], object detection [3, 17, 20, 21, 25], and segmentation [2, 10, 18]. Among them, object detection is a fundamental task which has already been extensively studied. Currently there are mainly two series of object detection frameworks: the two-stage frameworks such as Faster-RCNN [21] and R-FCN [3] which extract proposals, followed by per-proposal classification and regression; and the one-stage frameworks such as YOLO [20] and SSD [17], which apply object classifiers and regressors in a dense manner without objectness-based pruning. Both of them do classification and regression on a set of pre-computed anchors.

Previous single shot object detectors, such as SSD, use multiple convolutional layers to detect objects with different sizes and aspect ratios. SSD uses a backbone network

(e.g., VGG16) to generate a low level detection feature map. Based on that, several layers of object detection feature maps are built, learning semantic information in a hierarchical manner. Smaller objects are detected by lower layers while larger objects are detected by higher layers. However, the low level features usually only capture basic visual patterns without strong semantic information. This may cause two problems: small objects may not be detected well, and the quality of high level features is also damaged by the imperfect low level features.

In this paper, we aim to address the problem discussed above, by designing a novel single shot detection network, named **Detection with Enriched Semantics (DES)**, which consists of two branches, a detection branch and a segmentation branch. The detection branch is a typical single shot detector, which takes VGG16 as its backbone, and detect objects with multiple object detection feature maps in different layers. This is shown in the upper part of Figure 1.

The segmentation branch is used to augment the low level detection feature map with strong semantic information. It takes the low level detection feature map as input, to learn semantic segmentation supervised by bounding-box level segmentation ground-truth. Then it augments the low level detection features with its semantic meaningful features, as shown in the left lower part of Figure 1.

Figure 2 gives an illustration of this semantic augmentation process. After the original low level features (B) are activated by segmentation features (C), the augmented low level features (D) can capture both the basic visual pattern as well as the semantic information of the object. This can be considered as an attention process, where each channel of the original low level feature map is activated by a semantically meaningful attention map, to combine both basic visual pattern and semantically meaningful knowledge.

In addition to the segmentation branch attached to the low level detection feature map, we also employ a global activation module for higher level detection feature maps. It consists of several global activation blocks, as shown in the right lower corner of Figure 1. The global activation block can prune out the location information, and learn the

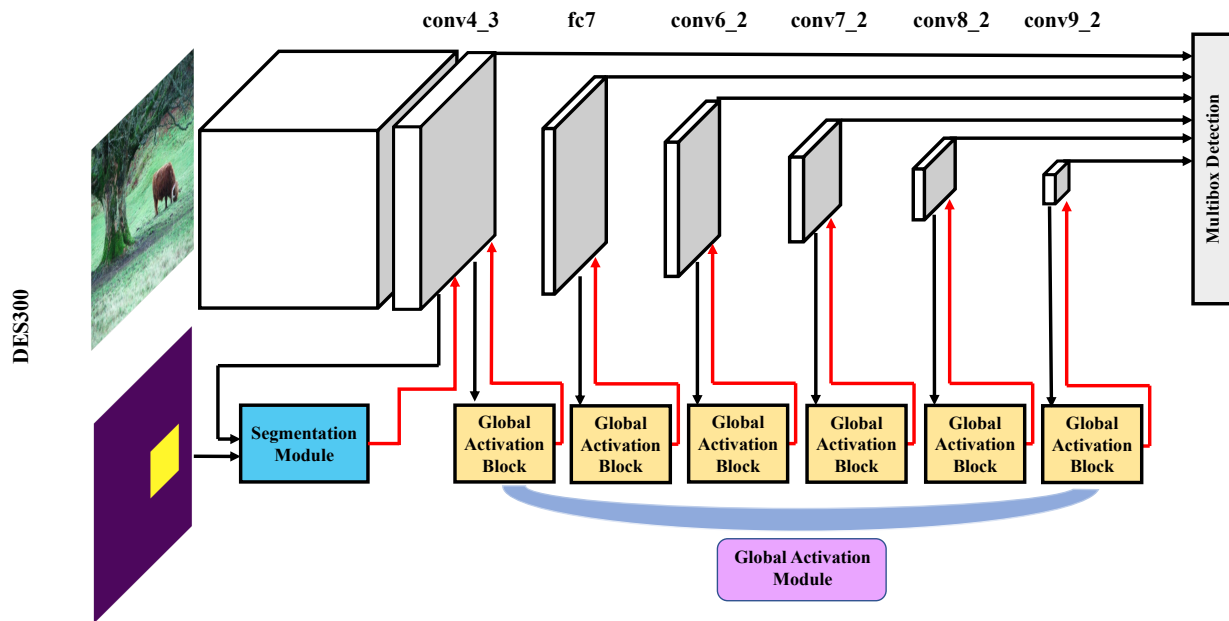


Figure 1. Pipeline for DES: the upper half is the object detection branch for DES which has six prediction source layers from *conv4\_3* up to *conv9\_2*; the lower half is the segmentation branch and the global activation module. The segmentation branch is added at the first prediction source layer *conv4\_3*. The global activation module consists of six global activation blocks. Those global activation blocks are added at each prediction source layer. The black arrows pointed to those modules are the input flow, and the red arrows pointed out from those modules are the output flow to replace the original feature map.

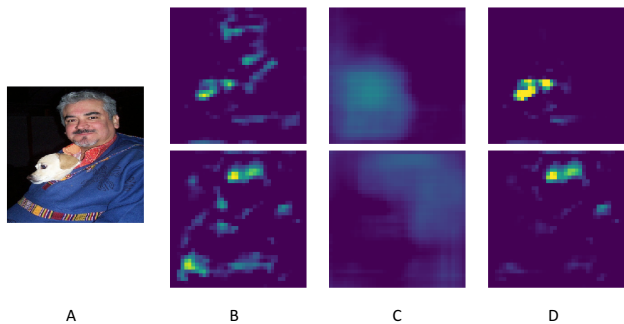


Figure 2. Low level features augmented with semantic meaningful features from the segmentation branch. A: original image fed into our detection network. B: original low level detection features ( $X$ ) for the input image. C: semantic meaningful features ( $Z$ ) from the segmentation branch. D: augmented low level features ( $X' = X \odot Z$ ) which is then used in the later stages for our detection network. We can see that  $X'$  can capture both basic visual pattern and high level semantic information.

relationship between channels and object classes in a self-supervised manner, which increases the semantic information of the object detection feature maps at higher layers.

We summarize our contributions as follows:

- We improve the typical deep single shot detectors by

enriching semantics, with a semantic segmentation branch to enhance low level detection features, and a global activation module to learn the semantic relationship between detection feature channels and object classes for higher level object detection features.

- We significantly improve the performance compared with popular single shot detectors. DES achieves an mAP of 81.7 on VOC2007 test and mAP of 32.8 on COCO test-dev.
- DES is time efficient. With a single Titan Xp GPU, it achieves 31.7 FPS, and is much faster than competitors like R-FCN and ResNet based SSD.

## 2. Related work

General object detection is a fundamental task in computer vision and has received lots of attention. Almost all the recent object detectors are based on deep networks. Generally there are two series of object detectors. The first series is the two-stage detectors. Some representative examples are R-CNN [8], Fast-RCNN [7], Faster-RCNN [21] and R-FCN [3]. These methods first generated a pool of object candidates, named object proposals, by a separate proposal generator such as Selective Search [26], Edge Boxes [28] or

Region Proposal Network (RPN), and then did per-proposal classification and bounding box regression.

Due to the speed limit of the two-stage frameworks, some research interest has been attracted by the series of one-stage object detectors, such as OverFeat [22], SSD [17] and YOLO [20]. These detectors eliminated the proposal generation, and did object detection and bounding box regression in a dense manner at different locations and scales.

However, all these methods take the object detection as the sole part in the training phase, without paying close attention to local cues at each position within the object, which happens to be semantic segmentation.

Semantic segmentation is another important vision task, which requires each pixel to be assigned to one of classes. General semantic segmentation methods such as DeepLab [2] and fully convolutional network (FCN) [18] need per-pixel labelling for the training. However, it has been shown that weakly annotated training data such as bounding boxes or image-level labels can also be utilized for semantic segmentation in [19].

We are not the first one to show segmentation information can be leveraged to help object detection [6, 10, 23]. Gidaris and Komodakis [6] used semantic segmentation-aware CNN features to augment detection features by concatenation at the highest level, but our work differs in a way that we put the segmentation information at the lowest detection feature map, and we use activation instead of concatenation to combine object detection features and segmentation features. He *et al.* [10] showed that multi-task training of object detection and instance segmentation can help to improve the object detection task with extra instance segmentation annotation, however, we do not consider extra annotation in our work. Another difference is how the segmentation branch is used. He *et al.* [10] train detection and segmentation in parallel, but our method uses segmentation features to activate the detection features.

Other work such as [14] has been done to improve object detectors by using top-down architecture to increase the semantic information. Our work achieves this in a simpler way, which does not involve reverse connections.

### 3. Proposed method

Detection with Enriched Semantics (DES) is a single-shot object detection network with three parts: a single shot detection branch, a segmentation branch to enrich semantics at low level detection layer, and a global activation module to enrich semantics at higher level detection layers.

We use SSD [17] as our single shot detection branch. SSD is built on top of a backbone which generates a low level detection feature map for object detection ( $conv4\_3$  for VGG16). Based on that, SSD builds a series of feature maps (*i.e.*,  $conv4\_3$  to  $conv9\_2$ ) to detect objects of small to large sizes, in a hierarchical manner, by applying anchors with

different sizes and aspect ratios on these feature maps.

In order to deal with the problems discussed previously, we employ a segmentation branch to augment low level detection features with semantic information. This segmentation branch is added at the first prediction source layer  $conv4\_3$ . General segmentation algorithms require pixel-level image annotation, but this is not feasible in the object detection task. Instead, we use bounding-box level weak segmentation labels to perform supervision for segmentation task. As shown in the left lower part in Figure 1, our segmentation branch takes  $conv4\_3$  as input, represented by the black arrow pointed from  $conv4\_3$  to segmentation branch. Then it generates a semantically augmented low level feature map  $conv4\_3'$ , which will be used for detection, represented by the red arrow pointed from segmentation module to  $conv4\_3$ . By employing segmentation branch, our network becomes a multi-task learning problem.

The feature map generated by the segmentation branch captures high level semantic information for each local area since the segmentation supervision pushes each local area to be assigned to one of the classes.

At higher level detection layers, the semantic information is already learned from previous layers; so it is not necessary to employ the segmentation branch for them. Further, since the resolution is smaller in higher levels, it will become harder to do the segmentation task based on them. Due to these reasons, we employ simple global activation blocks, on  $conv4\_3$  through  $conv9\_2$ , to enrich their semantic information in a self-supervised manner.

#### 3.1. Semantic enrichment at low level layer

Semantic enrichment at low level detection feature layer is achieved by the segmentation branch, which performs weakly supervised semantic segmentation. It takes the low level detection layer from the detection branch ( $conv4\_3$  for SSD300) and bounding-box level segmentation ground-truth as inputs, and generates a semantic meaningful feature map with the same dimension. Then this feature map is used to activate the input low level detection layer from the detection branch by element-wise multiplication.

Mathematically, let  $X \in \mathbb{R}^{C \times H \times W}$  be the low level detection feature map from the detection branch,  $G \in \{0, 1, 2, \dots, N\}^{H \times W}$  be the segmentation ground-truth where  $N$  is the number of classes (20 for VOC and 80 for COCO). The segmentation branch computes  $Y \in \mathbb{R}^{(N+1) \times H \times W}$  as the prediction of per-pixel segmentation where

$$Y = \mathcal{F}(G(X))$$

satisfying

$$Y \in [0, 1]^{(N+1) \times H \times W}, \sum_{c=0}^N Y_{c,h,w} = 1.$$

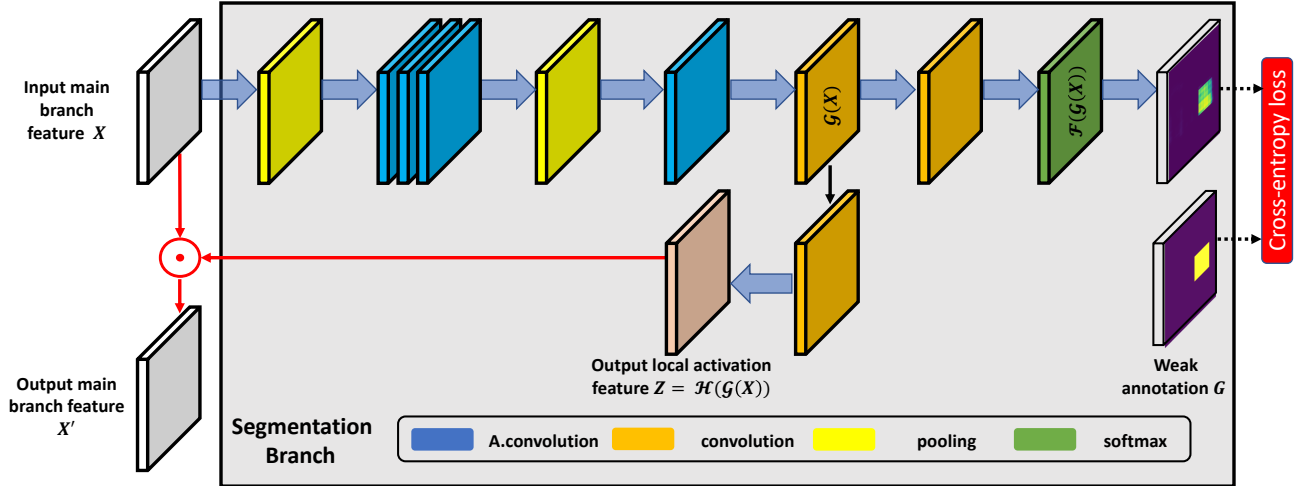


Figure 3. Segmentation branch takes an intermediate feature map from object detection branch (e.g. *conv4\_3* for SSD300) as input, which generates a semantically meaningful feature map  $Z$  to activate input  $X$  to be  $X'$ .  $X'$  is then used in the detection branch.

$\mathcal{G}(X) \in \mathbb{R}^{C' \times H \times W}$  is the intermediate result which will be further used to generate semantic meaningful feature map:

$$Z = \mathcal{H}(\mathcal{G}(X)) \in \mathbb{R}^{C \times H \times W}.$$

The semantic meaningful feature map  $Z$  is then used to activate the original low level detection feature map  $X$  by element-wise multiplication:  $X' = X \odot Z$ . where  $X'$  is the semantically activated low level detection feature map which conveys both basic visual patterns and high level semantic information.  $X'$  will replace the original  $X$  in the detection branch for object detection. Figure 3 gives an illustration of this process.

For the segmentation branch, we design a simple network branch mainly composed of atrous convolutional layers [2]. We add four atrous convolutional layers (noted as ‘A. convolution’ in Figure 3) with  $3 \times 3$  kernel size after the input feature map  $X$ . The first three atrous convolutional layers have a dilation rate of 2 and the last atrous convolutional layer has a dilation rate of 4. After that we deploy another  $1 \times 1$  convolutional layer to generate  $\mathcal{G}(X)$  mentioned above. This intermediate feature map has two functions: generate segmentation prediction  $Y = \mathcal{F}(\mathcal{G}(X))$  and provide high semantic information to activate the input feature map  $X' = X \odot \mathcal{H}(\mathcal{G}(X))$ . Towards this end, there are two paths attached to  $\mathcal{G}(X)$ . The first path ( $\mathcal{F}$  path) takes a  $1 \times 1$  convolution layer with  $N + 1$  output channels and a softmax layer to generate the segmentation prediction  $Y$ . The second path ( $\mathcal{H}$  path) takes another  $1 \times 1$  convolution layer whose output channel number equals the channel number of  $X$ , to generate a semantic meaningful feature map  $Z$  in order to activate the feature map in the detection branch by element-wise multiplication. We show an example of this activation process in Figure 2. Column A is the

input image and column B is one slice of the original low level object detection feature map  $X$ . We can notice that the semantic meaningful feature map  $Z$  generated by our segmentation branch can capture very high level semantic information (the dog or human information). The final activated feature map  $X'$  conveys both basic visual pattern and high level semantic information. All these layers keep the size of feature maps unchanged.

The final problem is how to generate segmentation ground-truth given only the object bounding boxes. The segmentation ground-truth  $G$  has the same resolution as the input layer of segmentation branch (*conv4\_3* for SSD300). We use a simple strategy to generate it: if a pixel  $G_{hw}$  locates within a bounding-box on the image lattice  $I$ , we assign the label of that bounding-box to  $G_{hw}$ ; if it locates within more than one bounding-boxes, we choose the label of the bounding-box with the smallest size; and if it does not locate in any bounding-box, we assign it to the background class. This strategy guarantees that there is only one class to be assigned to each pixel in  $G$ . We show an example of this weak segmentation ground-truth in Figure 4.

### 3.2. Semantic enrichment at higher level layers

In conjunction with our segmentation branch, we propose another module named global activation module at higher layers. It contains several global activation blocks, attached at each object detection source layer in the detection branch. Global activation blocks can learn the relationship between channels and object classes, by eliminating the spatial information, in a self-supervised manner.

The global activation module is shown in the right lower part of Figure 1, which consists of several global activation blocks attached to each of the object detection source layer



Figure 4. Example of weak segmentation ground-truth. Left: Input image with a size of  $300 \times 300$ , with a person and a horse. Right: Segmentation ground-truth for the left image, with a size of  $38 \times 38$ ; the pixels locate in both person and horse bounding-boxes will be assigned to person class since its bounding-box is smaller.

(i.e., *conv4\_3* up to *conv9\_2* for SSD300).

The global activation block consists of three stages: spatial pooling, channel-wise learning and broadcasted multiplying. Formally, given the input  $X \in \mathbb{R}^{C \times H \times W}$ , the spatial pooling stage will produce  $Z \in \mathbb{R}^C$  by

$$Z_i = \frac{1}{HW} \sum_{h,w} X_{ihw}$$

and the channel-wise learning stage will generate the activation feature

$$S = \text{Sigmoid}(W_2 \cdot \text{ReLU}(W_1 Z)) \in \mathbb{R}^{C \times 1 \times 1}$$

where  $W_2 \in \mathbb{R}^{C \times C'}$ ,  $W_1 \in \mathbb{R}^{C' \times C}$ . In the broadcasted multiplying stage,  $S$  is used to activate  $X$  to get  $X' \in \mathbb{R}^{C \times H \times W}$  where  $X'_{ihw} = X_{ihw} \cdot S_i$ . Finally, the  $X'$  will replace the original  $X$  in the detection branch. In our experiments, we keep  $C' = \frac{1}{4}C$  for all global activation blocks.

This architecture was used for image classification in [12]. Here we extend it for object detection.

### 3.3. Multi-task training

In the training phase, an extra cross-entropy loss function for segmentation task will be added in conjunction with the original object detection loss function  $L_{\text{det}}(I, B)$  where  $I$  is the image and  $B$  is the bounding-box annotation. Our new loss function is formulated as:

$$L_{\text{seg}}(I, G) = -\frac{1}{HW} \sum_{h,w} \log(Y_{G_{h,w,h,w}})$$

where  $Y \in [0, 1]^{(N+1) \times H \times W}$  is the segmentation prediction, and  $G \in \{0, 1, 2, \dots, N\}^{H \times W}$  is the segmentation ground-truth generated by bounding-box annotation, where  $N$  is the number of classes excluding background class.

By adding the new segmentation loss function to the original detection loss function, the final objective function

we are optimizing is:

$$L(I, B, G) = L_{\text{det}}(I, B) + \alpha L_{\text{seg}}(I, G)$$

where  $\alpha$  is a parameter to balance those two tasks.

## 4. Experiments

We present comprehensive experimental results on two main object detection datasets: PascalVOC [4] and MS COCO [16]. For PascalVOC, we follow the common split, which uses the union of VOC2007 *trainval* and VOC2012 *trainval* as the training data, and uses VOC2007 *test* as the test data. We also show the result on VOC2012 *test* with the model trained on the union of VOC2007 *trainvaltest* and VOC2012 *trainval*. For COCO, we use a popular split which takes *trainval35k* [1] for training, *minival* for validation, and we show results on *test-dev2017* which is evaluated on the official evaluation server.

For the basic object detection framework, we choose VGG16-based SSD300 [17] and SSD512 as our single shot detection branch. Note that SSD has been updated with a new data augmentation trick which boosts the performance with a huge gap. We follow the latest version of SSD with all those tricks. The segmentation branch is inserted at the first prediction source layer, i.e. *conv4\_3* for both SSD300 and SSD512. The global activation module consists of several global activation blocks, 6 for SSD300 and 7 for SSD512, and all of those blocks are added at each prediction source layer. For the first prediction source layer, the segmentation branch is inserted before the global activation block. We follow the SSD training strategy throughout our experiments, and set the trade-off parameter  $\alpha$  to be 0.1.

We will use the terminology ‘DES300’ and ‘DES512’ to represent our Detection with Enriched Semantics network built on VGG16-based SSD300 and SSD512 respectively in the rest of our paper.

### 4.1. Experiment on VOC

For the VOC dataset, we do the training on a machine with 2 Titan Xp GPUs. To focus on the effectiveness of our DES network, we keep the training settings used in SSD unchanged. We first train the model with  $\text{lr} = 10^{-3}$  for 80k iterations, and then continue the training with  $\text{lr} = 10^{-4}$  for 20k iterations and  $\text{lr} = 10^{-5}$  for another 20k iterations. The momentum is fixed to be 0.9 and the weight decay is set to be 0.0005. Those parameters are aligned with the original SSD experiments. We use pre-trained SSD model for VOC to initialize our model, and initialize the parameters in the first five layers of segmentation branch with the parameters of *conv5\_1*, *conv5\_2*, *conv5\_3*, *fc\_6* and *fc\_7* in the detection branch. The rest two convolutional layers of the segmentation branch are initialized by Xavier initialization [9]. We

| method                         | backbone  | mAP         | aero        | bike        | bird        | boat        | bottle      | bus         | car         | cat         | chair       | cow         | table       | dog         | horse       | mbike       | persn       | plant       | sheep       | sofa        | train       | tv          |
|--------------------------------|-----------|-------------|-------------|-------------|-------------|-------------|-------------|-------------|-------------|-------------|-------------|-------------|-------------|-------------|-------------|-------------|-------------|-------------|-------------|-------------|-------------|-------------|
| Fast [7]                       | VGG16     | 70.0        | 77.0        | 78.1        | 69.3        | 59.4        | 38.3        | 81.6        | 78.6        | 86.7        | 42.8        | 78.8        | 68.9        | 84.7        | 82.0        | 76.6        | 69.9        | 31.8        | 70.1        | 74.8        | 80.4        | 70.4        |
| Faster [21]                    | VGG16     | 73.2        | 76.5        | 79.0        | 70.9        | 65.5        | 52.1        | 83.1        | 84.7        | 86.4        | 52.0        | 81.9        | 65.7        | 84.8        | 84.6        | 77.5        | 76.7        | 38.8        | 73.6        | 73.9        | 83.0        | 72.6        |
| Faster [11]                    | ResNet101 | 76.4        | 79.8        | 80.7        | 76.2        | 68.3        | 55.9        | 85.1        | 85.3        | <b>89.8</b> | 56.7        | 87.8        | 69.4        | 88.3        | 88.9        | 80.9        | 78.4        | 41.7        | 78.6        | 79.8        | 85.3        | 72.0        |
| R-FCN [3]                      | ResNet101 | 80.5        | 79.9        | 87.2        | 81.5        | 72.0        | <b>69.8</b> | 86.8        | 88.5        | <b>89.8</b> | <b>67.0</b> | <b>88.1</b> | 74.5        | <b>89.8</b> | <b>90.6</b> | 79.9        | 81.2        | 53.7        | 81.8        | 81.5        | 85.9        | 79.9        |
| RON384++ [14]                  | VGG16     | 77.6        | 86.0        | 82.5        | 76.9        | 69.1        | 59.2        | 86.2        | 85.5        | 87.2        | 59.9        | 81.4        | 73.3        | 85.9        | 86.8        | 82.2        | 79.6        | 52.4        | 78.2        | 76.0        | 86.2        | 78.0        |
| Gidaris <i>et al.</i> [6]      | VGG16     | 78.2        | 80.3        | 84.1        | 78.5        | 70.8        | 68.5        | 88.0        | 85.9        | 87.8        | 60.3        | 85.2        | 73.7        | 87.2        | 86.5        | 85.0        | 76.4        | 48.5        | 76.3        | 75.5        | 85.0        | 81.0        |
| Shrivastava <i>et al.</i> [23] | VGG16     | 76.4        | 79.3        | 80.5        | 76.8        | 72.0        | 58.2        | 85.1        | 86.5        | 89.3        | 60.6        | 82.2        | 69.2        | 87.0        | 87.2        | 81.6        | 78.2        | 44.6        | 77.9        | 76.7        | 82.4        | 71.9        |
| SSD300 [17]                    | VGG16     | 77.5        | 79.5        | 83.9        | 76.0        | 69.6        | 50.5        | 87.0        | 85.7        | 88.1        | 60.3        | 81.5        | 77.0        | 86.1        | 87.5        | 84.0        | 79.4        | 52.3        | 77.9        | 79.5        | 87.6        | 76.8        |
| SSD321 [17]                    | ResNet101 | 77.1        | 76.3        | 84.6        | 79.3        | 64.6        | 47.2        | 85.4        | 84.0        | 88.8        | 60.1        | 82.6        | 76.9        | 86.7        | 87.2        | 85.4        | 79.1        | 50.8        | 77.2        | <b>82.6</b> | 87.3        | 76.6        |
| DES300 (Ours)                  | VGG16     | 79.7        | 83.5        | 86.0        | 78.1        | 74.8        | 53.4        | 87.9        | 87.3        | 88.6        | 64.0        | 83.8        | 77.2        | 85.9        | 88.6        | <b>87.5</b> | 80.8        | 57.3        | 80.2        | 80.4        | <b>88.5</b> | 79.5        |
| SSD512 [17]                    | VGG16     | 79.5        | 84.8        | 85.1        | 81.5        | 73.0        | 57.8        | 87.8        | 88.3        | 87.4        | 63.5        | 85.4        | 73.2        | 86.2        | 86.7        | 83.9        | 82.5        | 55.6        | 81.7        | 79.0        | 86.6        | 80.0        |
| SSD513 [17]                    | ResNet101 | 80.6        | 84.3        | <b>87.6</b> | 82.6        | 71.6        | 59.0        | 88.2        | 88.1        | 89.3        | 64.4        | 85.6        | 76.2        | 88.5        | 88.9        | <b>87.5</b> | 83.0        | 53.6        | 83.9        | 82.2        | 87.2        | <b>81.3</b> |
| DES512 (Ours)                  | VGG16     | <b>81.7</b> | <b>87.7</b> | 86.7        | <b>85.2</b> | <b>76.3</b> | 60.6        | <b>88.7</b> | <b>89.0</b> | 88.0        | <b>67.0</b> | 86.9        | <b>78.0</b> | 87.2        | 87.9        | 87.4        | <b>84.4</b> | <b>59.2</b> | <b>86.1</b> | 79.2        | 88.1        | 80.5        |

Table 1. Results on VOC2007 test. The first section contains some representative baselines [3, 7, 11, 14, 21], the second section contains other detectors exploiting segmentation information [6, 23], the third section contains low resolution SSD and DES, and the last section contains high resolution SSD and DES. Note that all these methods are trained on VOC2007 trainval and VOC2012 trainval.

| method                         | backbone  | mAP         | aero        | bike        | bird        | boat        | bottle      | bus         | car         | cat         | chair       | cow         | table       | dog         | horse       | mbike       | persn       | plant       | sheep       | sofa        | train       | tv          |
|--------------------------------|-----------|-------------|-------------|-------------|-------------|-------------|-------------|-------------|-------------|-------------|-------------|-------------|-------------|-------------|-------------|-------------|-------------|-------------|-------------|-------------|-------------|-------------|
| Faster [11]                    | ResNet101 | 73.8        | 86.5        | 81.6        | 77.2        | 58.0        | 51.0        | 78.6        | 76.6        | 93.2        | 48.6        | 80.4        | 59.0        | 92.1        | 85.3        | 84.8        | 80.7        | 48.1        | 77.3        | 66.5        | 84.7        | 65.6        |
| R-FCN [3]                      | ResNet101 | 77.6        | 86.9        | 83.4        | <b>81.5</b> | 63.8        | 62.4        | 81.6        | 81.1        | 93.1        | 58.0        | 83.8        | 60.8        | 92.7        | 86.0        | 84.6        | 84.4        | <b>59.0</b> | 80.8        | 68.6        | 86.1        | 72.9        |
| RON384++ [14]                  | VGG16     | 75.4        | 86.5        | 82.9        | 76.6        | 60.9        | 55.8        | 81.7        | 80.2        | 91.1        | 57.3        | 81.1        | 60.4        | 87.2        | 84.8        | 84.9        | 81.7        | 51.9        | 79.1        | 68.6        | 84.1        | 70.3        |
| Gidaris <i>et al.</i> [6]      | VGG16     | 73.9        | 85.5        | 82.9        | 76.6        | 57.8        | <b>62.7</b> | 79.4        | 77.2        | 86.6        | 55.0        | 79.1        | 62.2        | 87.0        | 83.4        | 84.7        | 78.9        | 45.3        | 73.4        | 65.8        | 80.3        | 74.0        |
| Shrivastava <i>et al.</i> [23] | VGG16     | 72.6        | 84.0        | 81.2        | 75.9        | 60.4        | 51.8        | 81.2        | 77.4        | 90.9        | 50.2        | 77.6        | 58.7        | 88.4        | 83.6        | 82.0        | 80.4        | 41.5        | 75.0        | 64.2        | 82.9        | 65.1        |
| SSD300 [17]                    | VGG16     | 75.8        | 88.1        | 82.9        | 74.4        | 61.9        | 47.6        | 82.7        | 78.8        | 91.5        | 58.1        | 80.0        | 64.1        | 89.4        | 85.7        | 85.5        | 82.6        | 50.2        | 79.8        | 73.6        | 86.6        | 72.1        |
| SSD321 [17]                    | ResNet101 | 75.4        | 87.9        | 82.9        | 73.7        | 61.5        | 45.3        | 81.4        | 75.6        | 92.6        | 57.4        | 78.3        | 65.0        | 90.8        | 86.8        | 85.8        | 81.5        | 50.3        | 78.1        | 75.3        | 85.2        | 72.5        |
| DES300 (Ours) <sup>1</sup>     | VGG16     | 77.1        | 88.5        | 84.4        | 76.0        | 65.0        | 50.1        | 83.1        | 79.7        | 92.1        | 61.3        | 81.4        | 65.8        | 89.6        | 85.9        | 86.2        | 83.2        | 51.2        | 81.4        | <b>76.0</b> | 88.4        | 73.3        |
| SSD512 [17]                    | VGG16     | 78.5        | 90.0        | 85.3        | 77.7        | 64.3        | 58.5        | 85.1        | 84.3        | 92.6        | 61.3        | 83.4        | 65.1        | 89.9        | 88.5        | 88.2        | 85.5        | 54.4        | 82.4        | 70.7        | 87.1        | 75.6        |
| SSD513 [17]                    | ResNet101 | 79.4        | 90.7        | 87.3        | 78.3        | 66.3        | 56.5        | 84.1        | 83.7        | <b>94.2</b> | 62.9        | <b>84.5</b> | 66.3        | <b>92.9</b> | 88.6        | 87.9        | 85.7        | 55.1        | 83.6        | 74.3        | 88.2        | 76.8        |
| DES512 (Ours) <sup>2</sup>     | VGG16     | <b>80.3</b> | <b>91.1</b> | <b>87.7</b> | 81.3        | <b>66.5</b> | 58.9        | <b>84.8</b> | <b>85.8</b> | 92.3        | <b>64.7</b> | 84.3        | <b>67.8</b> | 91.6        | <b>89.6</b> | <b>88.7</b> | <b>86.4</b> | 57.7        | <b>85.5</b> | 74.4        | <b>89.2</b> | <b>77.6</b> |

Table 2. Results on VOC2012 test. Note that all methods in this table are trained on VOC2007 trainvaltest and VOC2012 trainval, except Gidaris *et al.* is trained on VOC2007 trainval and VOC2012 trainval.

also do another experiment by resetting all the parameters after *conv6\_1* layer in the detection branch with Xavier initialization. This will lead to similar results compared with the current setting.

The results on VOC2007 test are shown in Table 1. DES outperforms original SSD on both resolution settings, and it improves the mAP from 77.5 to 79.7 and from 79.5 to 81.7 for low and high resolution respectively. Our VGG16-based model can even significantly outperform ResNet101-based SSD models, which are much deeper than VGG16, and this highlights the effectiveness of our method.

Compared with other baselines such as popular two-stage methods and other detector combined with segmentation, our DES still shows a significant performance improvement. For VOC2012 test results shown in Table 2, the same tendency remains. DES outperforms all the competitors with a large gap.

Table 3 summarizes the results when SSD and DES are fine-tuned from models trained on COCO. DES outperforms SSD on all test settings with a large margin. It shows our method can also get benefit from extra training data like the COCO dataset.

## 4.2. Experiment on COCO

We use the similar strategy for COCO task. The DES is implemented from the original SSD networks which have

| method      | backbone | 07 test | 12 test |
|-------------|----------|---------|---------|
| SSD300 [17] | VGG16    | 79.8    | 78.5    |
| DES300      | VGG16    | 82.7    | 81.0    |
| SSD512 [17] | VGG16    | 83.2    | 82.2    |
| DES512      | VGG16    | 84.3    | 83.7    |

Table 3. Results on VOC2007 test and VOC2012 test when detectors are fine-tuned from models pre-trained on COCO.

slightly different default box settings to fit COCO dataset. The training is conducted on the trainval135k generated from COCO trainval2014 dataset. We first train the network with lr =  $10^{-3}$  for 280k iterations, followed by training with lr =  $10^{-4}$  for 80k iteration and training with lr =  $10^{-5}$  for another 40k iteration. The momentum is set to be 0.9 and the weight decay is set to be 0.0005, which are consistent with the original SSD settings.

Similar to our methods used for VOC, we use the pre-trained SSD model for COCO to initialize our parameters, and use weights in *conv5\_1*, *conv5\_2*, *conv5\_3*, *fc\_6* and *fc\_7* to initialize the first five layers in the segmentation branch. However, different from VOC, we find that resetting weights after *conv6\_1* is crucial for good performance, and we can only get a small improvement around 0.2 for AP@0.5 if we keep those weights after *conv6\_1* same as the SSD pre-trained model.

We report results on COCO test-dev2017 with 20288 images from the official evaluation server deployed on CodaLab in Table 4. Compared with our baseline SSD,

<sup>1</sup><http://host.robots.ox.ac.uk:8080/anonymous/RCMS6B.html>

<sup>2</sup><http://host.robots.ox.ac.uk:8080/anonymous/OBE3UF.html>

| method                         | backbone  | data        | mAP  | AP50 | AP75 | APsml | APmdm | APlrg | ARI  | AR10 | AR100 | ARsml | ARmdm | ARlrg |
|--------------------------------|-----------|-------------|------|------|------|-------|-------|-------|------|------|-------|-------|-------|-------|
| Faster [21]                    | VGG16     | trainval    | 21.9 | 42.7 | -    | -     | -     | -     | -    | -    | -     | -     | -     | -     |
| Faster+++ [11]                 | ResNet101 | trainval    | 34.9 | 55.7 | -    | -     | -     | -     | -    | -    | -     | -     | -     | -     |
| R-FCN [3]                      | ResNet101 | trainval    | 29.9 | 51.9 | -    | 10.8  | 32.8  | 45.0  | -    | -    | -     | -     | -     | -     |
| RON384++ [14]                  | VGG16     | trainval    | 27.4 | 49.5 | 27.1 | -     | -     | -     | -    | -    | -     | -     | -     | -     |
| Shrivastava <i>et al.</i> [23] | VGG16     | trainval35k | 27.5 | 49.2 | 27.8 | 8.9   | 29.5  | 41.5  | 25.5 | 37.4 | 38.3  | 14.6  | 42.5  | 57.4  |
| SSD300 [17]                    | VGG16     | trainval35k | 25.1 | 43.1 | 25.8 | 6.6   | 25.9  | 41.4  | 23.7 | 35.1 | 37.2  | 11.2  | 40.4  | 58.4  |
| SSD321 [17]                    | ResNet101 | trainval35k | 28.0 | 45.4 | 29.3 | 6.2   | 28.3  | 49.3  | 25.9 | 37.8 | 39.9  | 11.5  | 43.3  | 64.9  |
| DES300 (Ours)                  | VGG16     | trainval35k | 28.3 | 47.3 | 29.4 | 8.5   | 29.9  | 45.2  | 25.6 | 38.3 | 40.7  | 14.1  | 44.7  | 62.0  |
| SSD512 [17]                    | VGG16     | trainval35k | 28.8 | 48.5 | 30.3 | 10.9  | 31.8  | 43.5  | 26.1 | 39.5 | 42.0  | 16.5  | 46.6  | 60.8  |
| SSD513 [17]                    | ResNet101 | trainval35k | 31.2 | 50.4 | 33.3 | 10.2  | 34.5  | 49.8  | 28.3 | 42.1 | 44.4  | 17.6  | 49.2  | 65.8  |
| DES512 (Ours)                  | VGG16     | trainval35k | 32.8 | 53.2 | 34.6 | 13.9  | 36.0  | 47.6  | 28.4 | 43.5 | 46.2  | 21.6  | 50.7  | 64.6  |

Table 4. Results on COCO *test-dev*. ‘sml’, ‘mdm’ and ‘lrg’ stand for small, medium and large respectively, and ‘mAP’, ‘AP50’ and ‘AP75’ mean average precision of IOU=0.5:0.95, IOU=0.5 and IOU=0.75 respectively. *trainval35k* is obtained by removing the 5k *minival* set from *trainval*.

our DES can provide huge improvement on all of the metrics. For the low resolution version (the third section in the table), we can achieve a relative improvement of 12.7% for mAP compared with baseline SSD300, from 25.1 to 28.3, and a significant relative improvement of 28.8% for small objects. For the high resolution version (the fourth section in the table), DES can improve the baseline from 28.8 to 32.8. Our DES can also outperform SSD based on ResNet101, which is deeper and much slower.

We can find that DES performs very good on small objects, outperforms at least 27.5% relatively compared with all other competitors which report performance on small objects. Although DES512 outperforms SSD512 based on VGG16 for detecting large objects, it is slightly worse than SSD513 based on ResNet101. We argue that SSD513 can benefit from ResNet101 which is much deeper, to detect large objects.

### 4.3. Discussion

#### 4.3.1 Architecture ablation and diagnosis

To further understand the effectiveness of our two extra modules, we do experiments with different settings and report the results in Table 5 on the VOC2007 *test* dataset based on DES300.

As can be seen from Table 5, the global activation module (G) can improve the performance by 0.6, which shows the effectiveness of global activation with global activation features. With the segmentation branch (S) added, the performance can be further improved with a large margin, which confirms our intuition that segmentation can be used to help object detection, and introducing high level semantic knowledge to the early stage of the detection network can contribute to a stronger object detector.

Another ablation study conducted is the weight of the segmentation loss. To do this, we train our DES network for VOC2007 *test* task with different  $\alpha$ ’s, *i.e.*, 0, 0.1 and 1. This hyper-parameter plays an important role for balancing object detection and segmentation tasks. Experiments shows that  $\alpha = 0.1$  yields the best performance, 0.3 better than  $\alpha = 0$  (eliminating segmentation loss) and 1.1 better

| method                        | mAP         |
|-------------------------------|-------------|
| SSD300                        | 77.5        |
| SSD300+G                      | 78.1        |
| SSD300+G+S ( $\alpha = 0.0$ ) | 79.4        |
| SSD300+G+S ( $\alpha = 0.1$ ) | <b>79.7</b> |
| SSD300+G+S ( $\alpha = 1.0$ ) | 78.6        |
| SSD300+G+S (in parallel)      | 78.2        |
| SSD300+G+DeeperVGG16          | 77.6        |

Table 5. Ablation result evaluated on VOC2007 *test* dataset. G stands for the global activation module and S stands for the segmentation branch.  $\alpha$  is the hyper-parameter controlling the trade-off between segmentation loss and detection loss discussed in Section 3.3.

than  $\alpha = 1$  (taking the tasks of object detection and segmentation equally important). This means the supervision over the segmentation task is important in our segmentation branch. But it should take less weight since the final task is object detection instead of segmentation, otherwise the segmentation module would lean toward the segmentation task too much and hurt the detection performance.

To further justify the effectiveness of our segmentation branch architecture, we conduct another two experiments. In the first experiment, we mimic Mask-RCNN [10] by training segmentation and detection branches in parallel, instead of using segmentation features to activate low level detection features. The improvement is very small (mAP of 78.2 as shown in the 6-th row in Table 5) and we believe the activation process is very important to improve detection features, and since our weak segmentation ground-truth does not contain extra information, it will not improve the performance significantly if trained in parallel. As a side evidence, we train two versions of Mask-RCNN, with no segmentation supervision and with weak segmentation supervision respectively, and the performance only goes up by a small amount of 0.6 on COCO *minival*. This indicates that Mask-RCNN cannot get a huge benefit from the weak segmentation supervision trained in parallel, and confirms our observation on DES. The second experiment we do is removing the segmentation loss and the activation process. Then the  $Z = \mathcal{H}(\mathcal{G}(X))$  is directly used by the ob-

| method      | backbond  | mAP  | time (ms/img) | FPS   | batchsize |
|-------------|-----------|------|---------------|-------|-----------|
| R-FCN [3]   | ResNet101 | 80.5 | 89.6          | 11.2  | 1         |
| SSD300 [17] | VGG16     | 77.5 | 9.2           | 109.3 | 8         |
| SSD321 [17] | ResNet101 | 77.1 | 33.2          | 30.2  | 8         |
| DES300      | VGG16     | 79.7 | 13.0          | 76.8  | 8         |
| SSD512 [17] | VGG16     | 79.5 | 18.6          | 53.8  | 8         |
| SSD513 [17] | ResNet101 | 80.6 | 61.6          | 16.2  | 8         |
| DES512      | VGG16     | 81.7 | 31.5          | 31.7  | 8         |

Table 6. Inference Speed of two-shot baseline R-FCN and single-shot SSD and DES under different resolutions. Here we report the mAP on VOC2007 *test* dataset in the mAP column, the time spent for inferring one image in milliseconds in the time column, as well as the number images processed within one second in the FPS column.

ject detection branch. This modification keeps the number of parameters introduced by our segmentation branch, and can be regraded as a ‘deeper VGG16’ with more parameters as the backbone. This architecture achieves an mAP of 77.6, which is much lower than our DES. This means the architecture of our segmentation branch is crucial, and the performance can be worse by naively adding more layers and parameters.

### 4.3.2 Inference Speed

To quantitatively evaluate the inference speed, we run DES, SSD, as well as R-FCN, on our machine with an NVIDIA Titan Xp GPU to compare the speed fairly.

All results are shown in Table 6. Note that to make comparison fair, we keep the batchsize to be the same in each comparison group (*i.e.* low resolution group based on SSD300 and the high resolution group based on SSD512). For ResNet101 based SSD321 and SSD513, we remove the batch normalization layer at the test time to reduce the run time and memory consumption following [5].

Our method is slower than original VGG16-based SSD due to our extra modules, however, DES is faster than ResNet101-based SSD with a large margin, and outperforms it in the meantime. DES300 has an FPS of 76.8 with mAP of 79.7, while DES512 achieves higher mAP with more inference time.

### 4.3.3 Detection examples

We show some detection examples in Figure 5. Left column is the result of original SSD300, and the right column is the result of our DES300. We show ‘aeroplane’ in the first two rows, and ‘pottedplant’ in the last row, for all detection results with a score higher than 0.3. From these examples, we can see that our method is good at detecting small objects like small aeroplanes and pottedplants, and it can also prune out some false positives which are incorrectly detected as aeroplane in the first row.

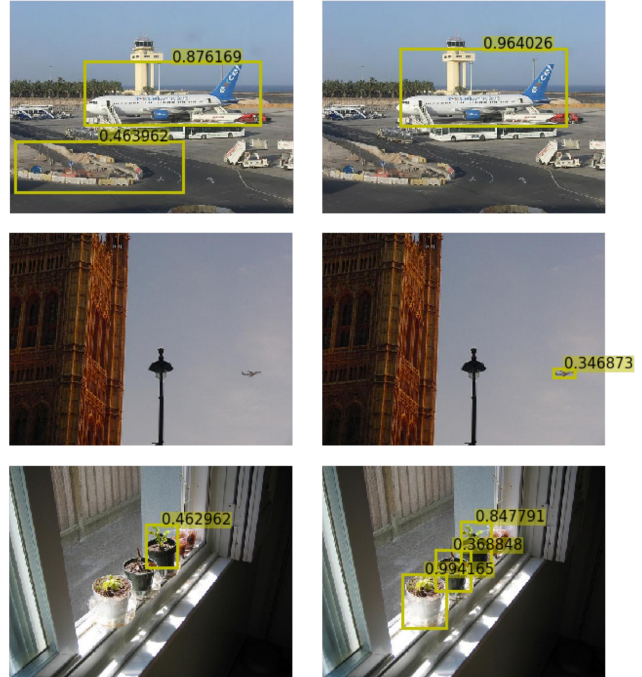


Figure 5. Examples of detection results. Left: Original SSD300. Right: DES300. See details in Section 4.3.3.

## 5. Conclusion

In this paper, we propose a novel single shot object detector named Detection with Enriched Semantics (DES). To address the problem that low level detection feature map does not have high level semantic information, we introduce a segmentation branch, which utilize the idea of weakly supervised semantic segmentation, to provide high semantic meaningful and class-aware features to activate and calibrate feature map used in the object detection. We also utilize a global activation module to provide global context information and pure channel-wise learning. Our method is flexible and simple, and does not require too much modifications to the original detection framework SSD. Quantitative evaluation shows our method excels in both accuracy and speed. Our method can also be applied to other two-stage or single shot object detectors, with stronger backbone, and we remain this as future work.

## Acknowledgements

This research was supported by ONR grant N00014-15-1-2356, the Center for Brains, Minds, and Machines (CBMM), funded by NSF STC award CCF-1231216, and the National Natural Science Foundation of China No. 61672336.

## References

- [1] S. Bell, C. Lawrence Zitnick, K. Bala, and R. Girshick. Inside-outside net: Detecting objects in context with skip pooling and recurrent neural networks. In *Proceedings of the IEEE Conference on Computer Vision and Pattern Recognition*, pages 2874–2883, 2016. [5](#)
- [2] L.-C. Chen, G. Papandreou, I. Kokkinos, K. Murphy, and A. L. Yuille. Deeplab: Semantic image segmentation with deep convolutional nets, atrous convolution, and fully connected crfs. *IEEE Transactions on Pattern Analysis and Machine Intelligence*, 2017. [1](#), [3](#), [4](#)
- [3] J. Dai, Y. Li, K. He, and J. Sun. R-fcn: Object detection via region-based fully convolutional networks. In *Advances in Neural Information Processing Systems*, pages 379–387, 2016. [1](#), [2](#), [6](#), [7](#), [8](#)
- [4] M. Everingham, L. Van Gool, C. K. Williams, J. Winn, and A. Zisserman. The pascal visual object classes (voc) challenge. *International journal of computer vision*, 88(2):303–338, 2010. [5](#)
- [5] C.-Y. Fu, W. Liu, A. Ranga, A. Tyagi, and A. C. Berg. Dssd: Deconvolutional single shot detector. *arXiv preprint arXiv:1701.06659*, 2017. [8](#)
- [6] S. Gidaris and N. Komodakis. Object detection via a multi-region and semantic segmentation-aware cnn model. In *Proceedings of the IEEE International Conference on Computer Vision*, pages 1134–1142, 2015. [3](#), [6](#)
- [7] R. Girshick. Fast r-cnn. In *Proceedings of the IEEE International Conference on Computer Vision*, pages 1440–1448, 2015. [2](#), [6](#)
- [8] R. Girshick, J. Donahue, T. Darrell, and J. Malik. Rich feature hierarchies for accurate object detection and semantic segmentation. In *Proceedings of the IEEE Conference on Computer Vision and Pattern Recognition*, pages 580–587, 2014. [2](#)
- [9] X. Glorot and Y. Bengio. Understanding the difficulty of training deep feedforward neural networks. In *Proceedings of the Thirteenth International Conference on Artificial Intelligence and Statistics*, pages 249–256, 2010. [5](#)
- [10] K. He, G. Gkioxari, P. Dollár, and R. Girshick. Mask r-cnn. In *Proceedings of the IEEE International Conference on Computer Vision*, 2017. [1](#), [3](#), [7](#)
- [11] K. He, X. Zhang, S. Ren, and J. Sun. Deep residual learning for image recognition. In *Proceedings of the IEEE Conference on Computer Vision and Pattern Recognition*, pages 770–778, 2016. [1](#), [6](#), [7](#)
- [12] J. Hu, L. Shen, and G. Sun. Squeeze-and-excitation networks. *arXiv preprint arXiv:1709.01507*, 2017. [5](#)
- [13] G. Huang, Z. Liu, L. van der Maaten, and K. Q. Weinberger. Densely connected convolutional networks. In *Proceedings of the IEEE Conference on Computer Vision and Pattern Recognition*, 2017. [1](#)
- [14] T. Kong, F. Sun, A. Yao, H. Liu, M. Lu, and Y. Chen. Ron: Reverse connection with objectness prior networks for object detection. In *IEEE Conference on Computer Vision and Pattern Recognition*, volume 1, page 2, 2017. [3](#), [6](#), [7](#)
- [15] A. Krizhevsky, I. Sutskever, and G. E. Hinton. Imagenet classification with deep convolutional neural networks. In *Advances in Neural Information Processing Systems*, pages 1097–1105, 2012. [1](#)
- [16] T.-Y. Lin, M. Maire, S. Belongie, J. Hays, P. Perona, D. Ramanan, P. Dollár, and C. L. Zitnick. Microsoft coco: Common objects in context. In *European Conference on Computer Vision*, pages 740–755. Springer, 2014. [5](#)
- [17] W. Liu, D. Anguelov, D. Erhan, C. Szegedy, S. Reed, C.-Y. Fu, and A. C. Berg. Ssd: Single shot multibox detector. In *European Conference on Computer Vision*, pages 21–37, 2016. [1](#), [3](#), [5](#), [6](#), [7](#), [8](#)
- [18] J. Long, E. Shelhamer, and T. Darrell. Fully convolutional networks for semantic segmentation. In *Proceedings of the IEEE Conference on Computer Vision and Pattern Recognition*, pages 3431–3440, 2015. [1](#), [3](#)
- [19] G. Papandreou, L.-C. Chen, K. P. Murphy, and A. L. Yuille. Weakly-and semi-supervised learning of a deep convolutional network for semantic image segmentation. In *Proceedings of the IEEE International Conference on Computer Vision*, pages 1742–1750, 2015. [3](#)
- [20] J. Redmon, S. Divvala, R. Girshick, and A. Farhadi. You only look once: Unified, real-time object detection. In *Proceedings of the IEEE Conference on Computer Vision and Pattern Recognition*, pages 779–788, 2016. [1](#), [3](#)
- [21] S. Ren, K. He, R. Girshick, and J. Sun. Faster r-cnn: Towards real-time object detection with region proposal networks. In *Advances in Neural Information Processing Systems*, pages 91–99, 2015. [1](#), [2](#), [6](#), [7](#)
- [22] P. Sermanet, D. Eigen, X. Zhang, M. Mathieu, R. Fergus, and Y. LeCun. Overfeat: Integrated recognition, localization and detection using convolutional networks. *arXiv preprint arXiv:1312.6229*, 2013. [3](#)
- [23] A. Shrivastava and A. Gupta. Contextual priming and feedback for faster r-cnn. In *European Conference on Computer Vision*, pages 330–348, 2016. [3](#), [6](#), [7](#)
- [24] K. Simonyan and A. Zisserman. Very deep convolutional networks for large-scale image recognition. *arXiv preprint arXiv:1409.1556*, 2014. [1](#)
- [25] P. Tang, X. Wang, X. Bai, and W. Liu. Multiple instance detection network with online instance classifier refinement. In *Proceedings of the IEEE Conference on Computer Vision and Pattern Recognition*, pages 2843–2851, 2017. [1](#)
- [26] J. R. Uijlings, K. E. Van De Sande, T. Gevers, and A. W. Smeulders. Selective search for object recognition. *International journal of computer vision*, 104(2):154–171, 2013. [2](#)
- [27] Y. Wang, L. Xie, C. Liu, S. Qiao, Y. Zhang, W. Zhang, Q. Tian, and A. Yuille. Sort: Second-order response transform for visual recognition. In *The IEEE International Conference on Computer Vision (ICCV)*, Oct 2017. [1](#)
- [28] C. L. Zitnick and P. Dollár. Edge boxes: Locating object proposals from edges. In *European Conference on Computer Vision*, pages 391–405. Springer, 2014. [2](#)